Physics Letters B 669 (2008) 223–228

Contents lists available at ScienceDirect

Physics Letters B

www.elsevier.com/locate/physletb

Study of the process $e^+e^- \to \omega\pi^0$ in the ϕ-meson mass region with the KLOE detector

KLOE Collaboration

F. Ambrosino [c,d], A. Antonelli [a], M. Antonelli [a], F. Archilli [h,i], P. Beltrame [b], G. Bencivenni [a], S. Bertolucci [a], C. Bini [f,g], C. Bloise [a], S. Bocchetta [j,k], F. Bossi [a], P. Branchini [k], P. Campana [a], G. Capon [a], T. Capussela [a], F. Ceradini [j,k], P. Ciambrone [a], F. Crucianelli [f], E. De Lucia [a], A. De Santis [f,g,*], P. De Simone [a], G. De Zorzi [f,g], A. Denig [b], A. Di Domenico [f,g], C. Di Donato [d], B. Di Micco [j,k], M. Dreucci [a], G. Felici [a], M.L. Ferrer [a], S. Fiore [f,g], P. Franzini [f,g], C. Gatti [a], P. Gauzzi [f,g], S. Giovannella [a], E. Graziani [k], W. Kluge [b], G. Lanfranchi [a], J. Lee-Franzini [a,l], D. Leone [b], M. Martini [a,e], P. Massarotti [c,d], S. Meola [c,d], S. Miscetti [a], M. Moulson [a], S. Müller [a], F. Murtas [a], M. Napolitano [c,d], F. Nguyen [j,k], M. Palutan [a], E. Pasqualucci [g], A. Passeri [k], V. Patera [a,e], F. Perfetto [c,d], P. Santangelo [a], B. Sciascia [a], A. Sciubba [a,e], A. Sibidanov [a], T. Spadaro [a], M. Testa [f,g], L. Tortora [k], P. Valente [g], G. Venanzoni [a], R. Versaci [a,e], G. Xu [a,m]

[a] *Laboratori Nazionali di Frascati dell'INFN, Frascati, Italy*
[b] *Institut für Experimentelle Kernphysik, Universität Karlsruhe, Germany*
[c] *Dipartimento di Scienze Fisiche dell'Università "Federico II", Napoli, Italy*
[d] *INFN Sezione di Napoli, Napoli, Italy*
[e] *Dipartimento di Energetica dell'Università "La Sapienza", Roma, Italy*
[f] *Dipartimento di Fisica dell'Università "La Sapienza", Roma, Italy*
[g] *INFN Sezione di Roma, Roma, Italy*
[h] *Dipartimento di Fisica dell'Università "Tor Vergata", Roma, Italy*
[i] *INFN Sezione di Roma Tor Vergata, Roma, Italy*
[j] *Dipartimento di Fisica dell'Università "Roma Tre", Roma, Italy*
[k] *INFN Sezione di Roma Tre, Roma, Italy*
[l] *Physics Department, State University of New York at Stony Brook, USA*
[m] *Institute of High Energy Physics of Academica Sinica, Beijing, China*

ARTICLE INFO

Article history:
Received 30 July 2008
Received in revised form 21 August 2008
Accepted 10 September 2008
Available online 7 October 2008
Editor: M. Doser

Keywords:
e^+e^- collisions
Rare ϕ decays
VMD
OZI violation
Isospin violation

ABSTRACT

We have studied the $e^+e^- \to \omega\pi^0$ cross section in the $\sqrt{s}$ interval 1000–1030 MeV using the $\pi^+\pi^-\pi^0\pi^0$ and $\pi^0\pi^0\gamma$ final states with a sample of ~ 600 pb^{-1} collected with the KLOE detector at DAΦNE. By fitting the observed interference pattern around M_ϕ for both final states, we extract the ratio of the decay widths $\Gamma(\omega \to \pi^0\gamma)/\Gamma(\omega \to \pi^+\pi^-\pi^0) = 0.0897 \pm 0.0016$ and derive the branching fractions $\mathrm{BR}(\omega \to \pi^+\pi^-\pi^0) = (90.24 \pm 0.19)\%$, $\mathrm{BR}(\omega \to \pi^0\gamma) = (8.09 \pm 0.14)\%$. The parameters describing the $e^+e^- \to \pi^+\pi^-\pi^0\pi^0$ reaction around M_ϕ are also used to extract the branching fraction for the OZI and G-parity violating $\phi \to \omega\pi^0$ decay: $\mathrm{BR}(\phi \to \omega\pi^0) = (4.4 \pm 0.6) \times 10^{-5}$.

1. Introduction

At low energy, below 1.4 GeV, the $e^+e^- \to \omega\pi^0$ cross section is largely dominated by the non-resonant processes $e^+e^- \to \rho/\rho' \to \omega\pi^0$. However, in the region around M_ϕ, a contribution from the OZI and G-parity violating decay $\phi \to \omega\pi^0$ is expected. This strongly suppressed decay ($\mathcal{O}(10^{-5})$) can be observed via interference with the non-resonant process, showing up as a dip in the total cross section dependence from $\sqrt{s}$.

The $e^+e^- \to \omega\pi^0$ cross section as a function of $\sqrt{s}$ is parametrized as [1]:

* Corresponding author.
E-mail addresses: antonio.desantis@roma1.infn.it (A. De Santis), simona.giovannella@lnf.infn.it (S. Giovannella).

0370-2693
doi:10.1016/j.physletb.2008.09.056

$$\sigma(\sqrt{s}) = \sigma_{nr}(\sqrt{s})\left|1 - Z\frac{M_\phi \Gamma_\phi}{D_\phi(\sqrt{s})}\right|^2, \quad (1)$$

where $\sigma_{nr}(\sqrt{s})$ is the bare cross section for the non-resonant process, Z is the interference parameter (i.e. the ratio between the ϕ decay and the non-resonant process amplitudes), while M_ϕ, Γ_ϕ and D_ϕ are the mass, the width and the inverse propagator of the ϕ meson respectively. The non-resonant cross section, in the energy range of interest, increases linearly with $\sqrt{s}$. A model independent parametrization is used to describe the non-resonant part: $\sigma_{nr}(\sqrt{s}) = \sigma_0 + \sigma'(\sqrt{s} - M_\phi)$.

In this work we study two different final states: $\pi^+\pi^-\pi^0\pi^0$ and $\pi^0\pi^0\gamma$, corresponding to the ω decay in $\pi^+\pi^-\pi^0$ and $\pi^0\gamma$, respectively. From the $\pi^+\pi^-\pi^0\pi^0$ analysis we have measured the Z parameter that has been used to determine the $\phi \to \omega\pi^0$ branching ratio (BR). In the case of $\pi^0\pi^0\gamma$ we expect contributions also from $\phi \to \rho\pi$ and $\phi \to S\gamma$ intermediate states, being S a scalar meson. In [2] we have shown that at $\sqrt{s} \sim M_\phi$ the interference between $\phi \to S\gamma$ and $e^+e^- \to \omega\pi^0$ events, evaluated by fitting the $M_{\pi\pi} - M_{\pi\gamma}$ Dalitz plot, is small. Therefore a fit to the cross section interference pattern for $\pi^0\pi^0\gamma$ final state will provide information about the $e^+e^- \to \rho/\rho' \to \omega\pi^0$ process and the resonant decays $\phi \to \omega\pi^0$ and $\phi \to \rho\pi^0$. Moreover, combining the results we extract the ratio $\Gamma(\omega \to \pi^0\gamma)/\Gamma(\omega \to \pi^+\pi^-\pi^0)$.

2. The KLOE detector

The KLOE experiment operates at DAΦNE [3], the Frascati ϕ-factory. DAΦNE is an e^+e^- collider running at a center of mass energy of ~ 1020 MeV, the mass of the ϕ meson. Equal energy positron and electron beams collide at an angle of $\pi - 25$ mrad, producing ϕ mesons nearly at rest.

The KLOE detector consists of a large cylindrical drift chamber, DC, surrounded by a lead-scintillating fiber electromagnetic calorimeter, EMC. A superconducting coil around the EMC provides a 0.52 T field. The drift chamber [4], 4 m in diameter and 3.3 m long, has 12,582 all-stereo tungsten sense wires and 37,746 aluminum field wires. The chamber shell is made of carbon fiber-epoxy composite and the gas used is a 90% helium, 10% isobutane mixture. These features maximize transparency to photons and reduce $K_L \to K_S$ regeneration and multiple scattering. The position resolutions are $\sigma_{xy} \sim 150$ μm and $\sigma_z \sim 2$ mm. The momentum resolution is $\sigma(p_\perp)/p_\perp \approx 0.4\%$. Vertices are reconstructed with a spatial resolution of ~ 3 mm. The calorimeter [5] is divided into a barrel and two endcaps, for a total of 88 modules, and covers 98% of the solid angle. The modules are read out at both ends by photomultipliers, both in amplitude and time. The readout granularity is $\sim (4.4 \times 4.4)$ cm^2, for a total of 2440 cells arranged in five layers. The energy deposits are obtained from the signal amplitude while the arrival times and the particles positions are obtained from the time differences. Cells close in time and space are grouped into calorimeter clusters. The cluster energy E is the sum of the cell energies. The cluster time T and position $\vec{R}$ are energy-weighed averages. Energy and time resolutions are $\sigma_E/E = 5.7\%/\sqrt{E\ (\mathrm{GeV})}$ and $\sigma_t = 57\ \mathrm{ps}/\sqrt{E\ (\mathrm{GeV})} \oplus 100$ ps, respectively. The KLOE trigger [6] uses both calorimeter and chamber information. In this analysis the events are selected by the calorimeter trigger, requiring two energy deposits with $E > 50$ MeV for the barrel and $E > 150$ MeV for the endcaps. A cosmic veto rejects events with at least two energy deposits above 30 MeV in the outermost calorimeter layer. Data are then analyzed by an event classification filter [7], which streams various categories of events in different output files.

3. Data analysis

All available statistics collected at the ϕ peak during 2001–2002 data-taking periods, corresponding to 450 pb^{-1}, have been analyzed. Moreover, four scan points (at 1010, 1018, 1023 and 1030 MeV) of ~ 10 pb^{-1} each and the off-peak run at 1000 MeV of ~ 100 pb^{-1} acquired in 2005–2006 have been included in this analysis. The luminosity is measured with 0.5% absolute precision counting large angle Bhabha scattering events [8]. Data taken at the ϕ peak are grouped in center of mass energy bins of 100 keV width. For all the other points, close $\sqrt{s}$ values are grouped together and the average center of mass energy is evaluated by weighting with luminosity.

In the following, the visible cross section for a given final state ($j = 4\pi, \pi\pi\gamma$) is defined $\sigma^j_{\mathrm{vis}} = N_j/\varepsilon_j L_{\mathrm{int}}$, where N_j, ε_j and L_{int}, are the number of signal events, the analysis efficiency and the luminosity, respectively.

The visible cross section is related to the bare cross section through the radiator function H (see Section 4):

$$\sigma^j_{\mathrm{vis}}(\sqrt{s}) = \int ds'\, H(s,s')\sigma^j(s') = \sigma^j(\sqrt{s}) * \delta^j_{\mathrm{rad}}(\sqrt{s}).$$

3.1. $e^+e^- \to \omega\pi^0 \to \pi^+\pi^-\pi^0\pi^0$

In the $\pi^+\pi^-\pi^0\pi^0$ analysis, data are filtered by selecting events with the expected final state signature: two tracks with opposite curvature connected to a vertex inside a small cylindrical fiducial volume ($\rho < 4$ cm and $|z| < 6$ cm) around the Interaction Point (IP) and four neutral clusters in the prompt Time Window (TW), defined as $|T_\gamma - R_\gamma/c| < \mathrm{MIN}(4\sigma_t, 2\ \mathrm{ns})$. To minimize contamination from machine background, we require for the clusters a minimal energy of 10 MeV and an angle with respect to the beam line in the interval $22^\circ \leqslant \theta_\gamma \leqslant 158^\circ$.

With this selection, at ϕ resonance, the main background contributions come from $\phi \to K_S K_L \to \pi^+\pi^-\pi^0\pi^0/\pi^0\pi^0\pi\mu\nu$ and $\phi \to K^+K^-$, with $K^\pm \to \pi^\pm\pi^0$, which have the same final state signature. Other two resonant background components ($\phi \to \eta\gamma$ with $\eta \to \pi^+\pi^-\pi^0$, and $\phi \to \pi^+\pi^-\pi^0$) mimic the final state signature because of additional clusters due to accidental coincidence of machine background events and/or shower fragments (cluster splitting). An additional non-resonant background contribution of the order of few percent from $e^+e^- \to \pi^+\pi^-\pi^0\pi^0$, dominated by the $a_1(1260)\pi$ intermediate state, is also expected for all $\sqrt{s}$ values [9].

A global kinematic fit ($N_{\mathrm{dof}} = 8$), imposing total four-momentum conservation and proper time of flight (TOF) for photons coming from the charged vertex, improves both the signal/background separation and the determination of the photon energies. The resulting χ^2 (χ^2_{Kfit}) is used to select signal enriched ($\chi^2_{\mathrm{Kfit}} < 50$), S_{evts}, and background dominated ($\chi^2_{\mathrm{Kfit}} > 50$), B_{evts}, samples. In S_{evts} sample the overall contamination from resonant background at $\sqrt{s} \sim M_\phi$ is about 12% while becomes negligible outside ϕ resonance. The contribution of the $a_1(1260)\pi$ background is about 4% for all $\sqrt{s}$ values. The signal selection efficiency in the S_{evts} sample is evaluated by Monte Carlo (MC) and corrected with data/MC ratios for tracking, vertexing and clustering. The resulting value $\varepsilon_{4\pi} \sim 38\%$ is dominated by the selection requirements and shows a small dependence on $\sqrt{s}$, which is taken into account in the evaluation of $\sigma^{4\pi}_{\mathrm{vis}}$.

The signal counting is performed for each $\sqrt{s}$ bin by fitting the π^0 recoil mass (M_{rec}) distribution for both, S_{evts} and B_{evts} samples with MC signal and resonant, non-resonant background shapes. The fit procedure is based on a likelihood function which takes into account both data and MC statistics. In Fig. 1(a)–(d), data-MC comparisons for events in the most populated bin of $\sqrt{s}$ are

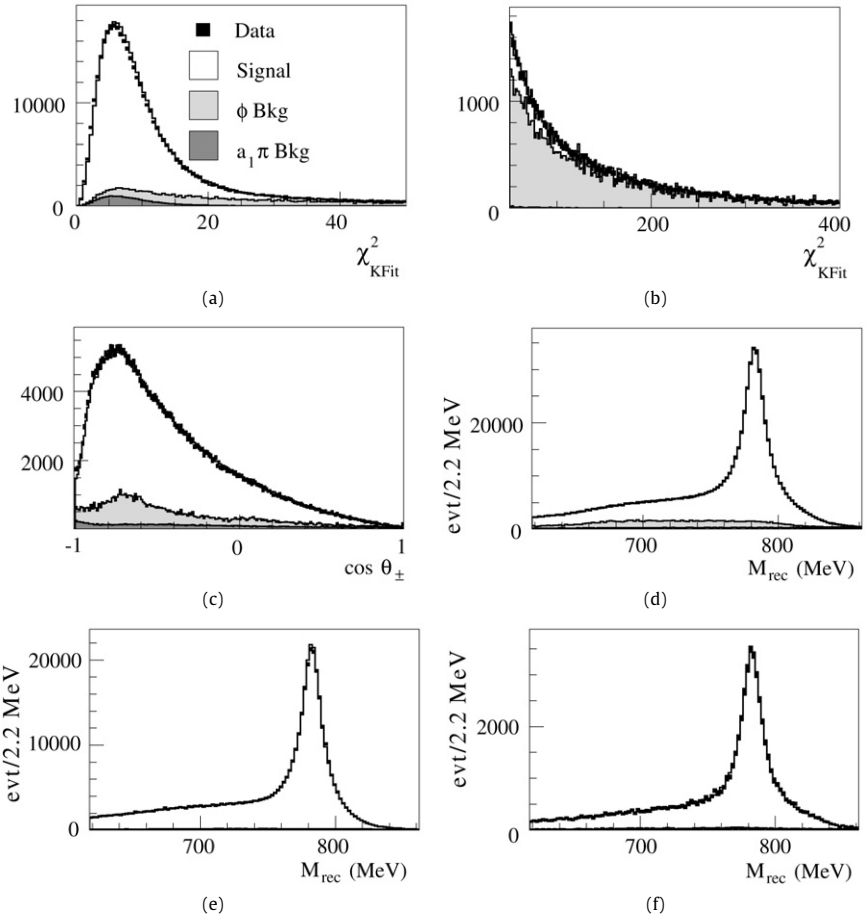

Fig. 1. Data-MC comparison for $\pi^+\pi^-\pi^0\pi^0$ events taken at $\sqrt{s} = 1019.75$ MeV: χ^2 of kinematic fit for $S_{\rm evts}$ (a) and $B_{\rm evts}$ (b) samples, angle between charged pions in the ω rest frame (c) and π^0 recoil mass (d) for $S_{\rm evts}$ events. The last distribution is shown also at $\sqrt{s} = 1000.10$ MeV (e) and $\sqrt{s} = 1029.95$ MeV (f).

Table 1
Signal counting, visible cross section and radiative correction for $e^+e^- \to \pi^+\pi^-\pi^0\pi^0$ and $e^+e^- \to \pi^0\pi^0\gamma$ events. The radiative correction values are calculated using for the bare cross section parameters in Table 2.

$\sqrt{s}$ (MeV)	$N^{4\pi}$	$\sigma^{4\pi}_{\rm vis}$ (nb)	$\delta^{4\pi}_{\rm rad}$	$N^{\pi\pi\gamma}$	$\sigma^{\pi\pi\gamma}_{\rm vis}$ (nb)	$\delta^{\pi\pi\gamma}_{\rm rad}$
1000.10	221 917±562	5.72 ± 0.05	0.885	27 110±167	0.550 ± 0.005	0.889
1009.90	25 968±173	6.20 ± 0.06	0.893	2958±56	0.581 ± 0.012	0.895
1017.20	16 209±171	5.71 ± 0.08	0.924	2108±46	0.564 ± 0.018	0.923
1018.15	22 167±158	5.60 ± 0.06	0.933	2557±60	0.541 ± 0.014	0.944
1019.30	4799±90	5.88 ± 0.12	0.918	322±22	0.480 ± 0.034	0.964
1019.45	58 077±340	5.89 ± 0.06	0.912	6058±101	0.497 ± 0.009	0.962
1019.55	93 596±445	5.93 ± 0.05	0.908	9516±130	0.487 ± 0.008	0.960
1019.65	171 571±888	5.98 ± 0.05	0.904	18 349±189	0.509 ± 0.007	0.958
1019.75	326 774±872	6.04 ± 0.05	0.900	34 049±282	0.505 ± 0.006	0.955
1019.85	256 008±1248	6.08 ± 0.05	0.896	26 124±234	0.508 ± 0.006	0.951
1019.95	35 850±263	6.20 ± 0.07	0.893	3510±74	0.491 ± 0.011	0.948
1020.05	17 971±167	6.21 ± 0.08	0.889	1843±52	0.516 ± 0.016	0.944
1020.15	8190±132	6.23 ± 0.11	0.886	702±32	0.501 ± 0.024	0.940
1020.45	9657±117	6.41 ± 0.09	0.878	667±31	0.488 ± 0.024	0.928
1022.30	16 931±141	7.24 ± 0.08	0.869	1891±43	0.612 ± 0.018	0.891
1023.00	29 611±177	7.41 ± 0.07	0.871	3101±61	0.619 ± 0.013	0.888
1029.95	33 681±186	7.84 ± 0.07	0.887	3896±65	0.689 ± 0.013	0.892

shown. In Fig. 1(e)–(f), the $M_{\rm rec}$ distribution is also shown for the two outermost center of mass energies.

The results are summarized in Table 1, where the signal counting ($N^{4\pi}$) and the visible cross section ($\sigma^{4\pi}_{\rm vis}$) are reported for all $\sqrt{s}$ bins. Errors on $\sigma^{4\pi}_{\rm vis}$ include statistics, background subtraction and a systematic error of 0.75%, dominated by the luminosity measurement (0.5%). The other systematics being due to cosmic ray veto, event counting and final state radiation.

We have checked the stability of the result by repeating the whole analysis chain with a wide variation of the selection criteria on: (a) minimum cluster energy and angle in the TW definition; (b) value of $\chi^2_{\rm Kfit}$ cut used to select $S_{\rm evts}$ and $B_{\rm evts}$ samples; (c) distribution used for the $B_{\rm evts}$ sample when performing signal counting; (d) data/MC efficiency correction curves. The resulting $\sigma^{4\pi}_{\rm vis}$ values are then used to estimate the systematic error of the measurement. The fit to the visible cross section as a function of $\sqrt{s}$ described in Section 4 is repeated for all of these variations. The quoted systematics uncertainty is calculated as the quadratic sum of RMS's obtained from variations (a)–(d).

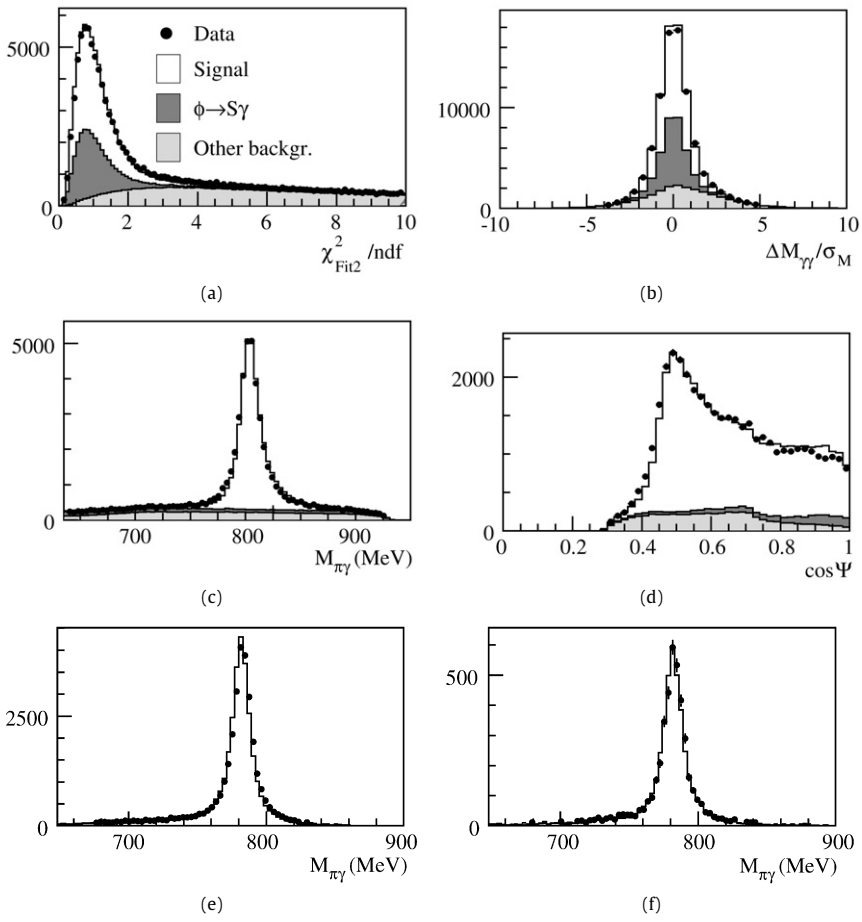

Fig. 2. Data-MC comparison for $\pi^0\pi^0\gamma$ events taken at $\sqrt{s} = 1019.75$ MeV: (a) normalized χ^2 of the second kinematic fit after acceptance cuts (Fit2), (b) normalized two-photon invariant mass after χ^2_{Fit2} cut, (c) $\pi^0\gamma$ invariant mass after $\Delta M_{\gamma\gamma}$ cut, (d) $\cos\psi$ distribution after all analysis cuts; $M_{\pi\gamma}$ distribution at $\sqrt{s} = 1000.10$ MeV (e) and $\sqrt{s} = 1029.95$ MeV (f).

3.2. $e^+e^- \to \omega\pi^0 \to \pi^0\pi^0\gamma$

The selection for $\pi^0\pi^0\gamma$ starts requiring five neutral clusters in the prompt Time Window with $E_\gamma \geqslant 7$ MeV and polar angle $|\cos\theta_\gamma| < 0.92$. After a first kinematic fit (Fit1, $N_{dof} = 9$) imposing total 4-momentum conservation and time of flight, photons are paired to π^0's by minimizing a χ^2 function, built using the invariant mass of the two $\gamma\gamma$ pairs. A second kinematic fit (Fit2, $N_{dof} = 11$) imposes also the constraint on π^0 masses.

The background is rejected by requiring $\chi^2_{Fit2}/Ndf \leqslant 5$ and $\Delta M_{\gamma\gamma} = |M_{\gamma\gamma} - M_\pi| \leqslant 5\sigma_{\gamma\gamma}$, where $M_{\gamma\gamma}$ and $\sigma_{\gamma\gamma}$ are evaluated using the photon momenta from Fit1. After these cuts the remaining sample is dominated by $e^+e^- \to \omega\pi^0 \to \pi^0\pi^0\gamma$ and $\phi \to S\gamma \to \pi^0\pi^0\gamma$ events. Signal is then selected neglecting the interference between these two processes and cutting on the intermediate state mass. Defining $M_{\pi\gamma}$ as the closest mass to M_ω of the two $\pi^0\gamma$ combinations, only events satisfying the requirement $750 < M_{\pi\gamma} < 830$ MeV are retained. The residual background contamination ($\sim 20\%$ at the ϕ peak) comes predominantly from $\phi \to \eta\gamma \to \pi^0\pi^0\pi^0\gamma$ events, where two photons are lost or merged.

In Fig. 2(a)–(d), data-MC comparison for events in the most populated $\sqrt{s}$ bin are shown. The ψ variable is the minimum angle between the photon and the π^0's in the di-pion rest frame. A good agreement is observed both after acceptance selection and after applying analysis cuts. The comparison for the $M_{\pi\gamma}$ distribution is also shown for the two outermost center of mass energies, where the background contribution is practically negligible (Fig. 2(e)–(f)).

The overall signal selection efficiency is evaluated by applying the whole analysis chain to signal MC events: $\varepsilon_{\pi\pi\gamma} \sim 46\%$, almost independent from $\sqrt{s}$. The value obtained for each bin, together with the corresponding integrated luminosity, has been applied to the signal counting to obtain the visible cross section ($\sigma_{vis}^{\pi\pi\gamma}$). Results are summarized in Table 1. Errors on $\sigma_{vis}^{\pi\pi\gamma}$ include statistics, background subtraction and a systematic error of 0.6%, dominated by the luminosity measurement (0.5%). The other systematic effects, related to cosmic ray veto and to the event classification filter, have been evaluated with downscaled data samples.

The stability of the results has been checked by repeating the fit with: (a) a variation of the selection criteria on the TW definition and on χ^2_{Fit2} and $M_{\pi\gamma}$ cuts; (b) a rescaling of the background components according to the value obtained by fitting background-enriched distributions on data with the corresponding MC components; (c) a subtraction to the visible cross section of the interference effect between $\phi \to S\gamma$ and the signal. This interference contribution is extracted from a fit to the Dalitz plot of the $\pi^0\pi^0\gamma$ final state [2] at the ϕ peak, which provides the parameters describing the two processes. These values are then used to evaluate for each $\sqrt{s}$ the interference contribution, which is subtracted to the corresponding $\sigma_{vis}^{\pi\pi\gamma}$. The largest contribution is 1.4%.

4. Fit results and ω branching ratios extraction

The measured values of visible cross section, shown in Table 1, are fitted with the parametrization (1) convoluted with the radiator function [10]. The free fit parameters of the bare cross section are: σ_0^j, $\Re e(Z_j)$, $\Im m(Z_j)$ and σ_j', where j represents either the 4π or $\pi\pi\gamma$ final state. In Fig. 3 data points with the superimposed fit result are shown for both channels. The values of the

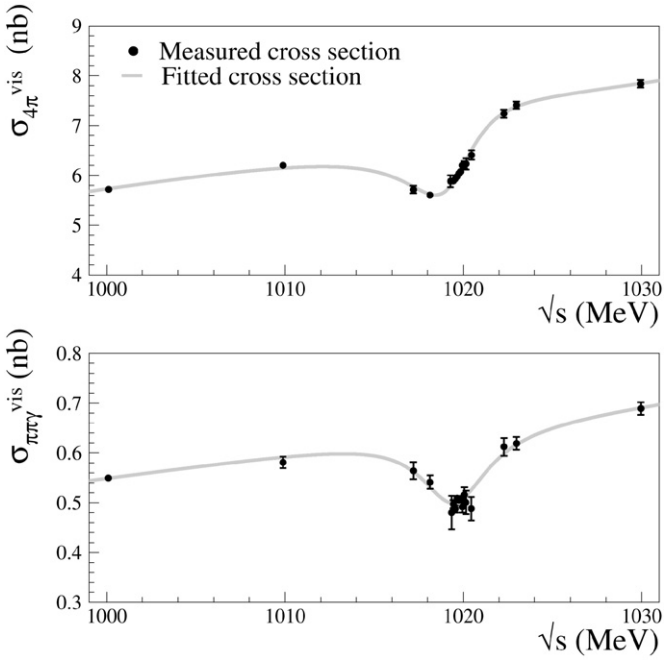

Fig. 3. Cross section fit results for the $e^+e^- \to \pi^+\pi^-\pi^0\pi^0$ (top) and $e^+e^- \to \pi^0\pi^0\gamma$ (bottom) channels. Black dots are data, solid line is the resulting fit function.

Table 2
Fit results for the $e^+e^- \to \pi^+\pi^-\pi^0\pi^0$ and for $e^+e^- \to \pi^0\pi^0\gamma$ cross section.

Parameter	$e^+e^- \to \pi^+\pi^-\pi^0\pi^0$	$e^+e^- \to \pi^0\pi^0\gamma$
σ_0 [nb]	$7.89 \pm 0.06 \pm 0.07$	$0.724 \pm 0.010 \pm 0.003$
$\Re e(Z)$	$0.106 \pm 0.007 \pm 0.004$	$0.011 \pm 0.015 \pm 0.006$
$\Im m(Z)$	$-0.103 \pm 0.004 \pm 0.003$	$-0.154 \pm 0.007 \pm 0.004$
σ' [nb/MeV]	$0.064 \pm 0.003 \pm 0.001$	$0.0053 \pm 0.0005 \pm 0.0002$

parameters are reported in Table 2. The second error quoted is the systematic uncertainty. It is evaluated as the quadratic sum of the RMS of the parameters extracted by repeating the fit with different conditions, as described in the previous section. The resulting $\chi^2/N_{\rm dof}$ are 11.79/13 ($P(\chi^2) = 54\%$) and 4.78/13 ($P(\chi^2) = 98\%$) for $\pi^0\pi^0\gamma$ and $\pi^+\pi^-\pi^0\pi^0$ channel, respectively. The fit has been repeated using a VMD model [1] based on ρ and ρ' intermediate states for the non-resonant term of the cross section. Results are in agreement with the linear parametrization within one standard deviation.[1]

After removing common systematics on the luminosity (0.5%), from the two measurements we obtain:

$$\frac{\sigma_0(\omega \to \pi^0\gamma)}{\sigma_0(\omega \to \pi^+\pi^-\pi^0)} = 0.0918 \pm 0.0016. \tag{2}$$

[1] The fitting function used for the non-resonant term is:

$$\sigma_{nr}^j(E) = \sigma_0^j \frac{m_\phi^3}{E^3} \frac{|m_\rho^2 \Pi_\rho(E) + A_j m_{\rho'}^2 \Pi_{\rho'}(E)|^2}{|m_\rho^2 \Pi_\rho(m_\phi) + A_j m_{\rho'}^2 \Pi_{\rho'}(m_\phi)|^2} \frac{P_{\rm f}(E)}{P_{\rm f}(m_\phi)},$$

where $\Pi_{\rho^{(\prime)}}(E) = (m_{\rho^{(\prime)}}^2 - E^2 - iE\Gamma_{\rho^{(\prime)}}(E))^{-1}$ is the vector meson propagator while $P_{\rm f}(E)$ describes the energy dependence of the phase space volume of the final state. For the latter we assume the approximation of an infinitely narrow ω meson. The free parameters in this case are σ_0^j and the real number A_j. This parametrization allows us to compare directly the value of σ_0^j obtained from this model with the value in Table 2. The width of the ρ meson has a dependence with energy $\Gamma_\rho(E) = \Gamma_\rho(m_\rho)(m_\rho/E)(p_\pi(E)/p_\pi(m_\rho))$, while the ρ' width is assumed fixed. $m_{\rho^{(\prime)}}$ and $\Gamma_{\rho^{(\prime)}}$ values are taken from [11]. For the parameter A we obtain: -0.15 ± 0.04, where the error takes into account only the contributions from Table 1.

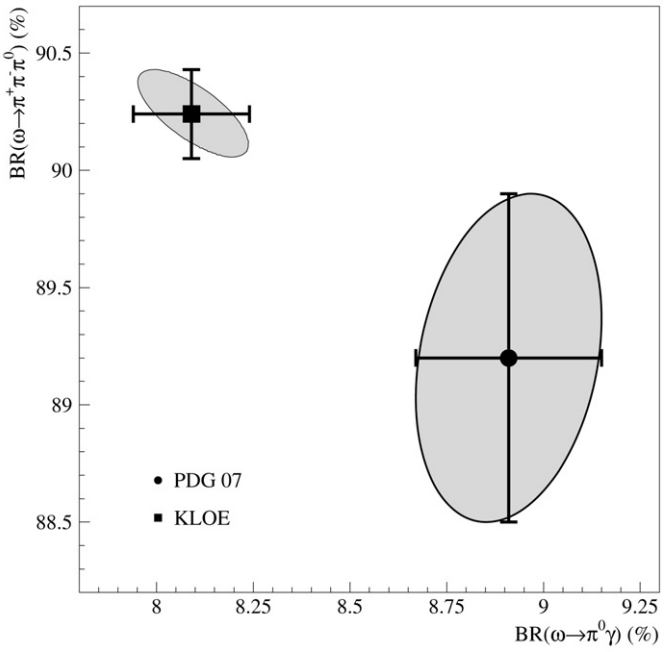

Fig. 4. Branching fraction for the two main ω decay channels. The black square is the KLOE fit result, while the black dot is the constrained fit result in [11]. The gray ellipses are the 68% C.L. regions.

Taking into account the phase space of the two decays [1], the ratio of the partial widths is:

$$\frac{\Gamma(\omega \to \pi^0\gamma)}{\Gamma(\omega \to \pi^+\pi^-\pi^0)} = 0.0897 \pm 0.0016. \tag{3}$$

Since these two final states account for 98% of the ω total width, we use the $\Gamma(\omega \to \pi^0\gamma)/\Gamma(\omega \to \pi^+\pi^-\pi^0)$ ratio and the sum of rarer BR's [11] to obtain from a fit:

$$\mathrm{BR}(\omega \to \pi^+\pi^-\pi^0) = (90.24 \pm 0.19)\%, \tag{4}$$

$$\mathrm{BR}(\omega \to \pi^0\gamma) = (8.09 \pm 0.14)\%, \tag{5}$$

with a correlation of -71%. Comparison between our evaluation and the values in [11] is shown in Fig. 4. Our result for BR($\omega \to \pi^0\gamma$) is less than the PDG value by three standard deviations. It is in good agreement with the recent prediction in [12].

5. BR($\phi \to \omega\pi^0$) evaluation

The measured $\sigma_0^{4\pi}$ and $Z_{4\pi}$ parameters of the $\pi^+\pi^-\pi^0\pi^0$ final state are related to the BR($\phi \to \omega\pi^0$) through the relation:

$$\mathrm{BR}(\phi \to \omega\pi^0) = \sigma_0(m_\phi)|Z_{4\pi}|^2 \frac{1}{\sigma_\phi} = \frac{\sigma_0^{4\pi}|Z_{4\pi}|^2}{\mathrm{BR}(\omega \to \pi^+\pi^-\pi^0)} \frac{M_\phi^2}{12\pi\,\Gamma(\phi \to e^+e^-)}, \tag{6}$$

where $\sigma_0(m_\phi)$ is the total cross section of the $e^+e^- \to \omega\pi^0$ process and σ_ϕ is the peak value of the bare cross section for the ϕ resonance. Using the parameters obtained from the $\pi^+\pi^-\pi^0\pi^0$ analysis, the Γ_{ee} measurement from KLOE [13] for the evaluation of σ_ϕ, and our value for BR($\omega \to \pi^+\pi^-\pi^0$) we extract:

$$\mathrm{BR}(\phi \to \omega\pi^0) = (4.4 \pm 0.6) \times 10^{-5}. \tag{7}$$

The error is reduced by a factor of two with respect to the best previous measurement from the SND experiment [1], which is in agreement with our result.

6. Conclusions

Using a sample of 600 pb^{-1} collected at center of mass energy between 1000 and 1030 MeV, we have measured the cross section parameters for the two processes $e^+e^- \to \pi^+\pi^-\pi^0\pi^0$ and $e^+e^- \to \pi^0\pi^0\gamma$, obtaining the ratio $\Gamma(\omega \to \pi^0\gamma)/\Gamma(\omega \to \pi^+\pi^-\pi^0)$ with an accuracy of 1.8%. This ratio, together with the unitarity relation and the BR measurements on the other ω decay channels, substantially improves the accuracy on the dominant ω branching fractions giving a value for BR$(\omega \to \pi^0\gamma)$ which is three standard deviations lower than the Particle Data Group fit [11]. Moreover, the parameters describing the $e^+e^- \to \pi^+\pi^-\pi^0\pi^0$ reaction around M_ϕ are used to extract the most precise BR measurement of the OZI and G-parity violating decay $\phi \to \omega\pi^0$.

Acknowledgements

We thank the DAΦNE team for their efforts in maintaining low background running conditions and their collaboration during all data-taking. We want to thank our technical staff: G.F. Fortugno and F. Sborzacchi for their dedicated work to ensure an efficient operation of the KLOE Computing Center; M. Anelli for his continuous support to the gas system and the safety of the detector; A. Balla, M. Gatta, G. Corradi and G. Papalino for the maintenance of the electronics; M. Santoni, G. Paoluzzi and R. Rosellini for the general support to the detector; C. Piscitelli for his help during major maintenance periods. This work was supported in part by EURODAPHNE, contract FMRX-CT98-0169; by the German Federal Ministry of Education and Research (BMBF) contract 06-KA-957; by the German Research Foundation (DFG), 'Emmy Noether Programme', contracts DE839/1-4; and by the EU Integrated Infrastructure Initiative Hadron Physics Project under contract number RII3-CT-2004-506078.

References

[1] V.M. Aulchenko, et al., J. Exp. Theor. Phys. 90 (2000) 927.
[2] KLOE Collaboration, F. Ambrosino, et al., Eur. Phys. J. C 49 (2007) 473.
[3] S. Guiducci, et al., in: P. Lucas, S. Webber (Eds.), Proceedings of the 2001 Particle Accelerator Conference, Chicago, IL, 2001, p. 353.
[4] KLOE Collaboration, M. Adinolfi, et al., Nucl. Instrum. Methods A 488 (2002) 51.
[5] KLOE Collaboration, M. Adinolfi, et al., Nucl. Instrum. Methods A 482 (2002) 363.
[6] KLOE Collaboration, M. Adinolfi, et al., Nucl. Instrum. Methods A 492 (2002) 134.
[7] KLOE Collaboration, F. Ambrosino, et al., Nucl. Instrum. Methods A 534 (2004) 403.
[8] KLOE Collaboration, F. Ambrosino, et al., Eur. Phys. J. C 47 (2006) 589.
[9] R.R. Akhmetshin, et al., Phys. Lett. B 466 (1999) 392.
[10] M. Greco, et al., Phys. Lett. B 318 (1993) 635.
[11] W.M. Yao, et al., J. Phys. G 33 (2006) 1, and 2007 partial update for 2008 edition, http://pdg.web.cern.ch/pdg.
[12] M. Benayoun, et al., Eur. Phys. J. C 55 (2008) 199.
[13] KLOE Collaboration, F. Ambrosino, et al., Phys. Lett. B 608 (2005) 199.